Analysis of SWAN Model with In-situ and Remotely Sensed Data From SandyDuck '97

W. Erick Rogers[1], Paul A. Hwang[1], David W. Wang[1], and James M. Kaihatu[1]

Abstract

In this paper, we present an analysis of a phase-averaged wind-wave model using a hindcast simulation of a moderate wave growth event that occurred during the SandyDuck '97 field experiment. We observe the activity of various source/sink terms in the model, with special attention to the deep-water dissipation term. We note shortcomings with this term and discuss possible improvements.

1. Introduction

The third generation wave action model SWAN ("Simulating WAves Nearshore", e.g., Booij et al., 1999) has been publicly available since 1997, but is still under active development. The accuracy of source/sink terms is, of course, a primary concern. The SandyDuck experiment, conducted from Sept. 22 to Oct. 31 1997 provides a wealth of data that can be used for analyzing the performance of source/sink mechanisms in this and other wave models. Wave data sources include two NDBC buoys (44014 at the 47m depth contour and buoy 44004 off the continental shelf), an array of pressure gages at 8 m depth, and a set of remotely sensed data from airborne lidar. The lidar data is of particular interest, as it is a novel form of wave data which provides high resolution free surface measurements. The time period during which lidar measurements were taken (1200 to 1600 UTC, Sept. 24 1997) includes a period of active wind wave growth and a period of decay, as well as a weak swell component. Thus, it is ideal for inferring activity of wave energy source/sink processes and studying corresponding formulae in the wave model.

This study emphasizes wave transformation at relatively large geographic scales: the primary model is run on a 300 km x 519 km grid, extending from the shoreline to open ocean beyond the shelf break.

[1] Oceanography Division, Naval Research Laboratory, Stennis Space Center, MS 39529; rogers@nrlssc.navy.mil

2. Wave data available

The SandyDuck ’97 field experiment yielded a wide variety of wave data. However, not all of this data were available to the public at the time of this model investigation. Below, we describe the data sources that were available and used in this investigation, noting that as more data is publicized, additional comparisons to the model results can be made. The locations of the instruments described are shown in Fig. 1.

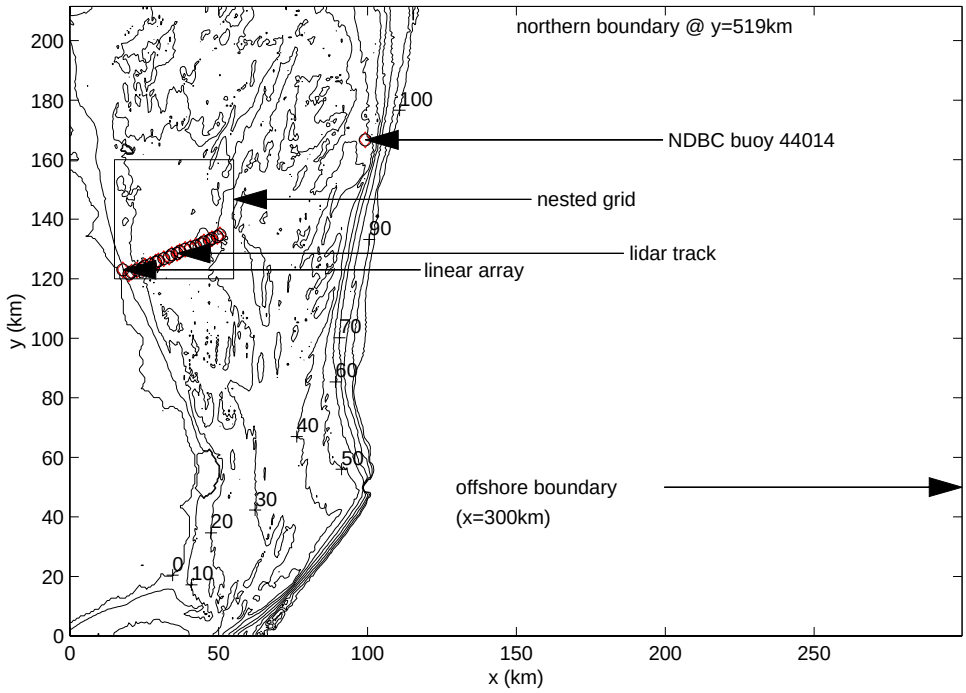

Figure 1. Bathymetry of the Duck, NC region (depths shown in meters); also shown are data collection locations and descriptions of model computational grid boundaries.

2.1 NDBC buoy 44014

This buoy, located at approximately 47m water depth, is the furthest offshore data source used for comparison to model output. This buoy is equipped for measurement/approximation of directional characteristics of the wave climate. The data is available continuously, processed on an hourly basis.

2.2 Lidar

The airborne scanning lidar system deployed for the experiment acquires the free surface topography of the ocean, from which wavenumber spectra can be directly computed. The accuracy of this type of directional data has been verified by Hwang et al. (2000a, b). In this case, the lidar data were collected along a 33 km cross-shore profile (~5 to 40 m depth). These data were taken during the time period of 1200 to 1400 UTC.

2.3 Linear array

The U.S. Army Corps of Engineers Field Research Facility maintains an array of 15 pressure gages for wave data measurement, located at approximately 8m water depth. The data is continuous and is processed every three hours.

3. Environmental conditions

3.1 Wind

Wind data at NDBC buoy 44014 for the time period of interest are shown, along with data from two other buoys in the region, in Fig. 2. (Buoy 44009 is approximately 209 km north of buoy 44014, and buoy 44004 is approximately 360 km east of 44009.). The data indicates considerable non-uniformity in the wind field prior to 0500 UTC Sept. 24, at which time winds are predominately offshore. Around this time, a frontal system passes over buoy 44014, and the winds there accelerate from weak (~3 m/s) to moderately strong (~10 m/s). The winds hold steady at this speed for approximately 8 hours, and comparison to the other two buoys shows that the wind field is fairly homogeneous during this period. The winds rotate clockwise continuously.

3.2 Swell

A mild background swell is fairly steady throughout the period of interest (Sept. 23-24). The period of the swell is 8-9 seconds, and the wave height at 44014 is well below 1 meter during the swell dominant (low wind) period prior to 0500 UTC Sept. 24.

4. The wave model

We use the third generation wave model SWAN (Booij et al. 1999). This model is comparable to WAM (WAMDI Group 1988), with additional physics for nearshore application, as well as a numerical scheme which makes it more efficient for computations at high geographic resolutions. (We note that the authors of SWAN discourage its application at scales larger than approximately 25km, due to severe numerical diffusion, but Rogers et al. (1999) have demonstrated that the effect of numerical diffusion is negligible for applications similar to this SandyDuck hindcast.)

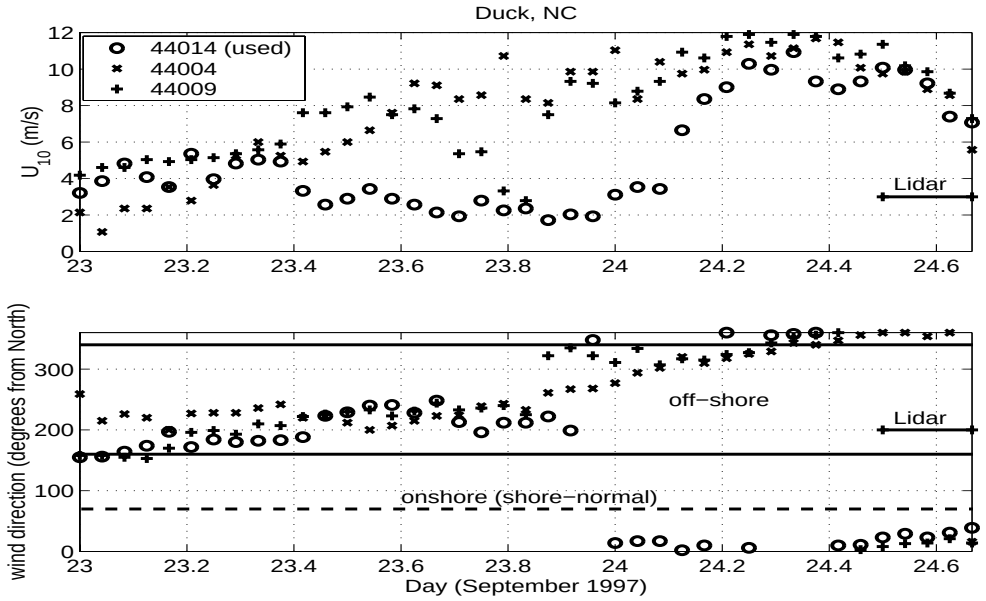

Figure 2. Wind data collected from three NDBC buoys in the region during the hindcast period. The time period of the lidar data collection is indicated.

4.1 Governing equation

The governing equation of SWAN (and similar models) is of the form

$$\frac{\partial N}{\partial t} + C_g \bullet \nabla N = \frac{S_{in} + S_{dis} + S_{nl}}{\sigma}, \qquad (1)$$

where N is the wave action density, which is the wave energy density divided by the relative frequency: $N(x,y,\theta,\sigma) = E(x,y,\theta,\sigma)/\sigma$, C_g is the wave group velocity for propagation in x,y,θ, and σ space, S_{in} is input from wind, S_{dis} is dissipation by steepness-limited breaking, sometime referred to as whitecapping (and by additional processes in shallow water), and S_{nl} represents nonlinear interactions (quadruplets and triads, the latter being significant only in shallow water).

4.2 S_{dis}

SWAN uses the formulation for steepness-limited deep-water dissipation of Hasselmann (1974) and Komen et al. (1984):

$$S_{dis}(\sigma,\theta) = -C_{ds}\left(\frac{\tilde{s}}{\tilde{s}_{PM}}\right)^m \tilde{\sigma}\left(\frac{k(\sigma)}{\tilde{k}}\right)^n E(\sigma,\theta), \qquad (2)$$

where C_{ds} is a coefficient of proportionality, $\tilde{s}$ is the overall wave steepness, $\tilde{s}_{PM}$ is the steepness of the idealized fully-developed (infinite fetch and duration) wave spectrum of Pierson and Moskowitz (1964), m and n are free parameters, $\tilde{\sigma}$ is the mean relative frequency of the entire spectrum, and $\tilde{k}$ is the mean wavenumber of the spectrum.

4.2.1 Standard formulation

Komen et al. (1984), determine the "best" C_{ds} and n to achieve the Pierson-Moskowitz spectrum. They suggest n=1. C_{ds} is dependent on the definition of $\tilde{\sigma}$ and $\tilde{k}$ used, so we will not discuss the actual value (for sake of brevity). With the existing whitecapping procedure, this same dissipation formula is applied to all spectral components, even though intuitively one would expect that sea and swell are dissipated by very different physical processes.

4.2.2 Modifications

Rogers et al. (2000) discuss two modest modifications to the standard dissipation formulation, meant to correct underprediction of low frequency energy which was consistently observed in hindcasts. We summarize below:

1) Higher value of n.

By repeating the Komen et al. (1984) tuning process, it can be shown that the "ideal" value of n for achieving the Pierson-Moskowitz limiting condition is between 1 and 1.5. Using a value of n greater than unity would have the effect of increasing dissipation on higher frequencies, while decreasing the dissipation of lower frequencies. Note that increasing n requires a corresponding increase in C_{ds} in order for the model to achieve stable growth under duration- and fetch-unlimited conditions. Through numerical experiments, we find that for n=1.5, C_{ds} must be increased by a factor of 1.9 to achieve this asymptote. This retuning of C_{ds} unfortunately will often lead to underprediction of total energy under more realistic (i.e. fetch- or duration-limited) conditions.

2) Swell dissipation.

It can be argued that swell should not be dissipated by the same mechanism by which wind sea is dissipated (i.e. steepness-limited breaking). Indeed, it is debatable as to whether swell is dissipated significantly by *any* process. The first step toward treating the dissipation of sea and swell differently would be to deactivate the dissipation of swell. The mechanism described in (2) can subsequently be replaced by another mechanism (e.g. an eddy viscosity formulation). This leaves the question of "how does one define swell?". One option would be to base this on the wave age used by the model's S_{in} formulation. For example, in the case of SWAN, which uses the Komen et al. (1984) formulation for wind input, S_{in}, if

$$28\frac{U_*}{c}\cos(\theta_{wv}-\theta_{wd})<\psi\,, \qquad (3)$$

then that particular wave component (described by c and θ_{wv}) would be considered swell. (Here, U_* is the friction velocity, c is the wave phase speed, θ_{wv} is the wave direction, and θ_{wd} is the wind direction.) With a value of ψ=1.0, any wave component which is not being actively forced by S_{in} would be considered swell. A

value of ψ<1.0 would be more conservative (would have a less drastic impact on model results).

Other methods of separating sea and swell exist which might also be used, e.g. those used by Tolman and Chalikov (1996) and Wang and Hwang (2000). We note that there exists a another, similar problem with the dissipation term which can be improved via separation of sea and swell: the presence of swell can lower the overall steepness, thereby (non-physically) reducing the dissipation of wind sea (see, e.g., Vledder 1999).

5. Model setup

5.1 Bathymetry

The original bathymetric grid is 1.4° longitude × 1.9° latitude, at 6 second resolution. It was created from a combination of NOS (National Ocean Service) hydrographic survey data and surveys conducted by researchers during the Duck '94 experiment (Herbers et al. 2000). The grid was artificially extended to the north and east and converted to a Cartesian coordinate system, with the (southwest) origin at 75.942 ° W, 35.08° N (Fig. 1).

Two computational grids were used:

1) Primary grid
   - purpose: to model wind-wave generation with sufficient fetch and to allow sufficient duration to propagate swell across this fetch.
   - resolution: $\Delta x = \Delta y = 2$km
   - size: 300km east-west; 519km north-south
   - duration: 0000UTC Sept. 23 – 1600UTC Sept. 24
2) Nested grid
   - purpose: to better resolve the bathymetry in intermediate and shallow depths (8-30m), and thus more accurately model depth-associated processes.
   - resolution: $\Delta x = 125$m; $\Delta y = 200$m
   - size: 40km east-west; 40km north-south
   - duration: 0300UTC Sept. 24 – 1600UTC Sept. 24

5.2 Wind

For wind forcing, we use data collected by NDBC buoy 44014. Thus wind forcing is nonstationary (time-varying) and uniform. Of course, if winds are non-homogeneous, then these wind speeds are less valid further from buoy 44014. However, (speaking of winds more that 100km distant from the buoy) only onshore- and alongshore- directed winds will have significant impact on waves in the region of interest (via wave propagation). It is evident in Fig. 2 that these winds are only mildly inhomogeneous, so wave predictions for the region of interest (say within ~100km of the buoy) should be valid with this assumption.

5.3 Swell

Some wave energy is observed in the data which was generated outside the computational grid. This must be represented in the model via open boundary input. As mentioned earlier, this swell is fairly constant during the two days of the simulation (Sept. 23 and 24), with T_p=8-9sec for the swell component, and H_{m0}=0.6-0.7m during the swell-dominant phase.

In preliminary simulations, data from NDBC buoy 44004 (450km offshore) were used for boundary input. However, since this buoy is not equipped for collecting directional data, a directional distribution had to be assumed via a time-averaging of directional distributions of the swell measured at the nearshore buoy (44014).

In simulations presented here, we take a simpler approach of a constant swell input, using a time-averaging of non-directional spectra at the offshore buoy (44004). The reason for using constant swell is simple: we are not particularly interested in modeling swell propagation accurately in this hindcast; of much greater interest is the effect that wind sea has on swell (in the model). Thus if we observe a decrease in the model's swell energy, we can say with certainty that this is due to the model formulation, not due to time-variation of model boundary input.

6. Results and analysis

6.1 Cross-shore variation of bulk parameters

Fig. 3 shows the cross-shore variation of two bulk parameters, peak wavenumber and variance (spectral energy level) at the period of time corresponding to the lidar data (1200-1400 UTC Sept. 24). Results without bottom friction are also presented. The effect of shoaling on the peak wavenumber is clearly seen in the data. This shift is also seen in the model, but appears to occur too early and too gradually.

Modeled variance is in excellent agreement with the data (note that variance is proportional to wave height squared, so error is exaggerated relative to traditional wave height comparison). However, there is a consistent high bias in wavenumber. If the error were due to inaccurate (low) wind forcing, an underprediction of variance would also be evident. Since this is not the case, it appears that wind forcing is not a primary source of error. This suggests that the source/sink terms in the model are biased toward higher frequencies.

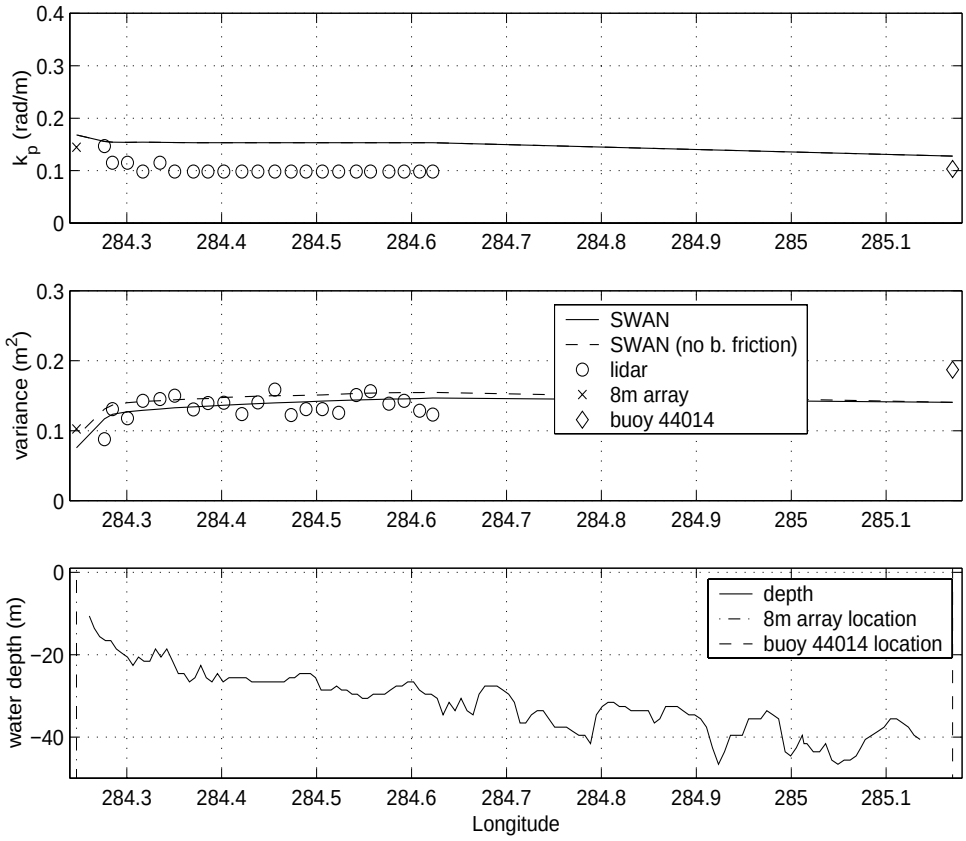

Figure 3. Comparison of SWAN to lidar and other data over a cross-shore transect, at approximately 1300 UTC 24 Sept. 1997. Model results with and without bottom friction are shown.

6.2 Temporal variation of bulk parameters

In Fig. 4, temporal variation at NDBC buoy 44014 is presented. In the T_{mean} comparison, we again see a bias toward higher frequencies, and that total energy (reflected by H_{m0}) is predicted fairly well. Directional spreading of the wind sea is predicted remarkably well, especially considering that this aspect of model performance is so often neglected in wave modeling research.

Using a higher value for n in the dissipation function has the expected effect of lowering the mean frequency (and therefore reducing error in this case) by shifting dissipation toward higher frequencies. However, due to the necessary retuning of C_{ds} (discussed above), total energy of the wind sea is less well predicted using n=1.5.

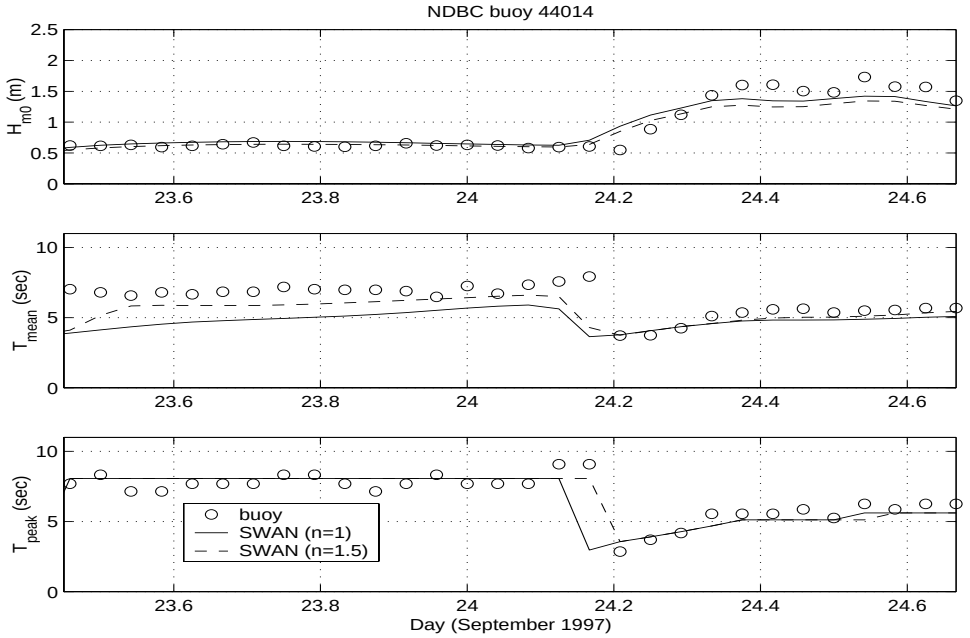

(a)

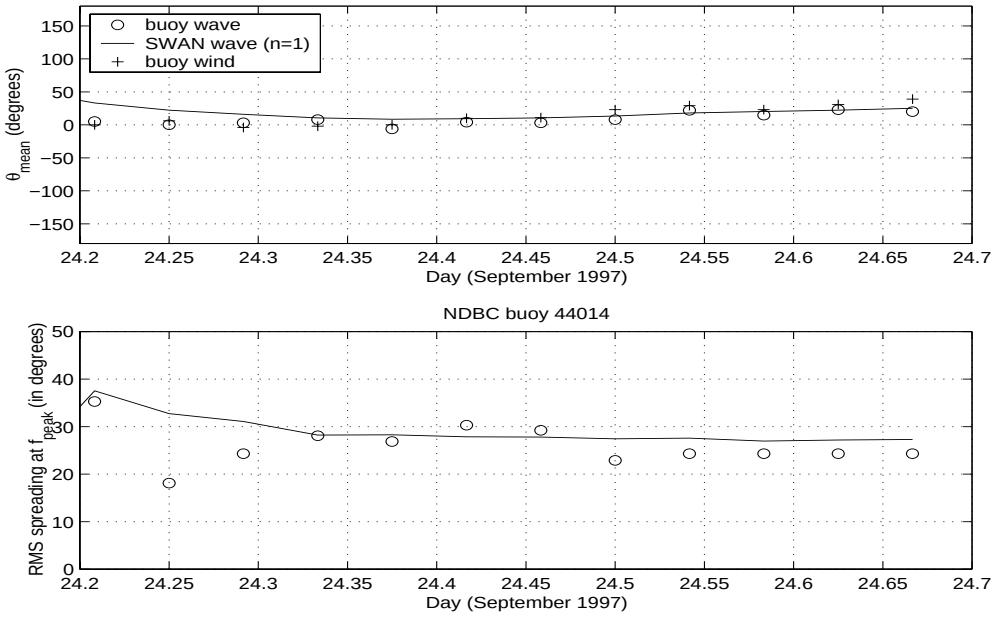

(b)

Figure 4. Time series comparison of bulk parameters (SWAN vs. measured data): at NDBC buoy 44014: 0000 UTC 23 Sept. - 1600 UTC 24 Sept. 1997. a) non-directional parameters, b) directional parameters. The mean period, T_{mean}, is calculated as the inverse of the centroid of the frequency spectrum between 0.07 Hz and 0.4 Hz.

6.3 Temporal variation of frequency spectra

6.3.1 "Blind" modeling results

By comparing temporal variation at individual frequencies, we can get a clearer indication of where the error occurs (Fig. 5). In general, the use of a higher n value in (2) produces only modest differences in energy level, though the change is almost always an improvement. At lower frequencies, dissipation is less with n=1.5; near the peak, the higher C_{ds} reduces energy slightly; at higher frequencies, the higher n and C_{ds} both contribute to greater dissipation, as one would expect.

Two items are of particular interest. The first is the behavior of the lowest frequency shown here (0.1 Hz) when the wind sea event occurs: a significant decrease in the model's energy at this frequency is observed. The decrease is due to the mean steepness term, $\tilde{s}$, in (2). When the wind sea arrives, the mean steepness of the spectrum increases, and therefore S_{ds} (as it is applied to the entire spectrum, including 0.1 Hz) increases. This is clearly nonphysical; one cannot expect the existence of wind sea to have this drastic an impact on swell frequencies over such short time/space scales. And indeed, in the buoy data, we see that low frequency energy (0.1 Hz) actually increases during this time (this may or may not be related to the wind event).

The second item of interest is model's underprediction of energy at frequencies below 0.2 Hz during the wind event. It is difficult to say with great certainty that this is due to inaccuracy of S_{dis}, and not S_{in} or S_{nl}. We do, however, feel that this is most likely the case.

6.3.2 Results without swell dissipation

If a model were to properly handle the dissipation of swell as a process distinct from the dissipation of wind sea, what impact would this have on results? By disallowing the breaking of swell using a method such as (3), we can gain some insight into this question. For this case, we do not need to be concerned with how swell *does* dissipate, since we can safely assume that swell does not dissipate significantly at the short time/space scales of this problem. The more difficult problem is how to separate the sea and swell. We experiment with (3), using a ψ value of 0.4. We note that this value is not chosen independently of the problem (unlike our choice of n and C_{ds} above), and the experiment is therefore useful for demonstrative purposes only.

These results are shown in Fig. 6. We immediately notice that 1) there is no artificial decrease in 0.1Hz energy during the wind event with the experimental model, and 2) at intermediate frequencies (0.12-0.19Hz) energy is not dissipated as quickly once is ceases to receive energy from the wind, generally correcting the underprediction of energy at these frequencies. However, at 0.14Hz, we see that the "correction" overshoots the data. This could be due to an overactive S_{in} term (which had previously been compensated by the overactive S_{dis} term), or perhaps it is due to a shortcoming in how we define swell. Clearly, this idea of reducing/preventing

the dissipation of swell needs further refinement. Further, we note that there are certain situations where swell might be expected to break/dissipate. A generally applicable dissipation term would need to address this.

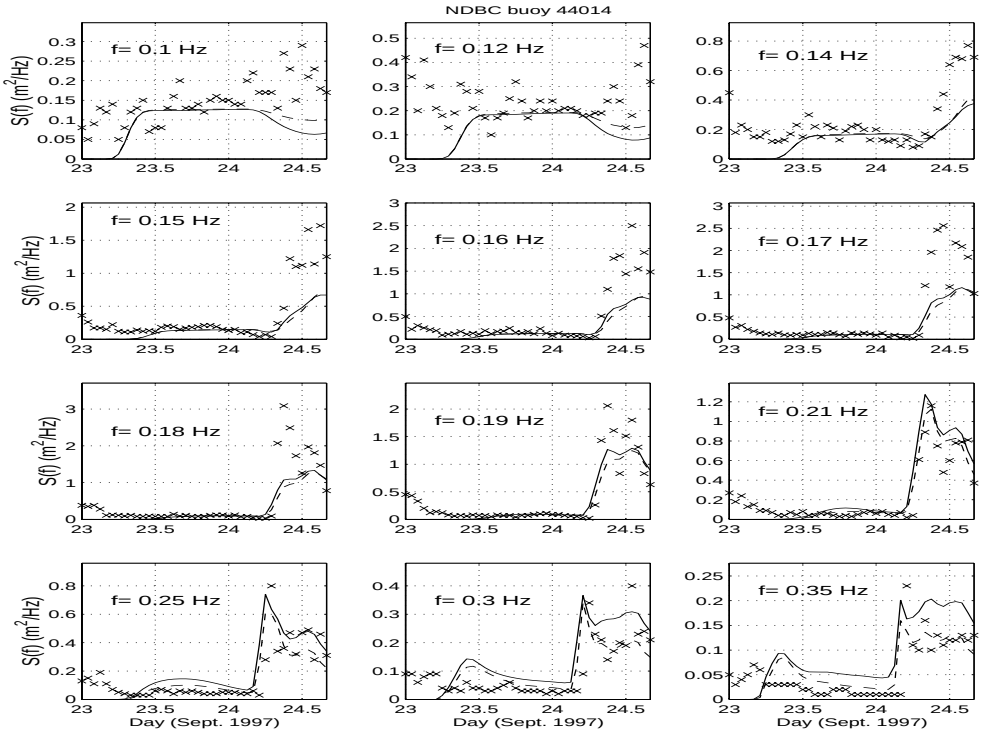

Figure 5. Comparison of SWAN frequency spectra time series to data from NDBC buoy 44014. "x": data; solid line: model with n=1; dashed line: model with n=1.5.

6.4 Geographic resolution

A numerical modeler often asks such questions as "Is the grid resolution affecting the accuracy of the computation?" or "Could the same answer be achieved with a less expensive (i.e. lower resolution) grid?". We can gain some insight into this "grid convergence" issue for our simulation by comparing the coarse grid simulation with the nested simulation. One can expect that resolution will have the greatest effect in shallow water, where waves react most to changes in the bathymetry. Therefore, we look for resolution-effects at the most shallow location in our grid, the 8m array (Fig. 7). This comparison indicates that the 2km resolution is quite adequate for this case, even as close to shore as the 8m array! Undoubtedly, however, this result is very case-specific: typical nearshore bathymetries are much less regular than that of Duck, N.C., and therefore a wave model would be more sensitive to the geographic resolution of computations.

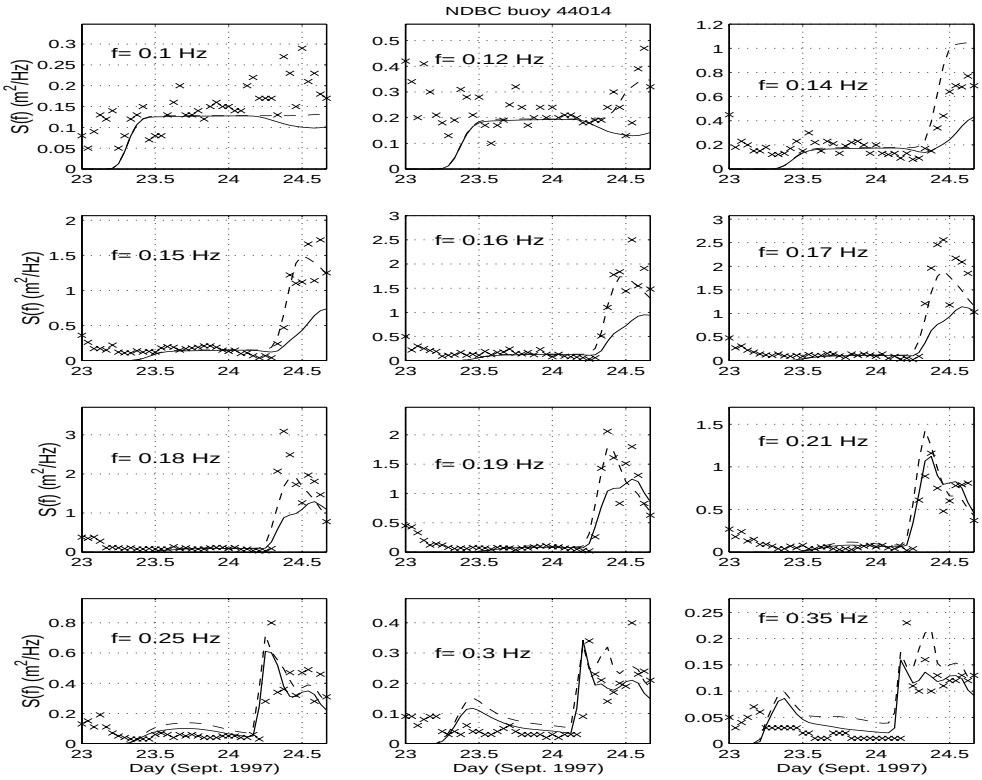

Figure 6. Comparison of SWAN frequency spectra time series to data from NDBC buoy 44014. "x": data; solid line: model with n=1.5; dashed line: model with n=1.5, without breaking of swell, as defined in (3).

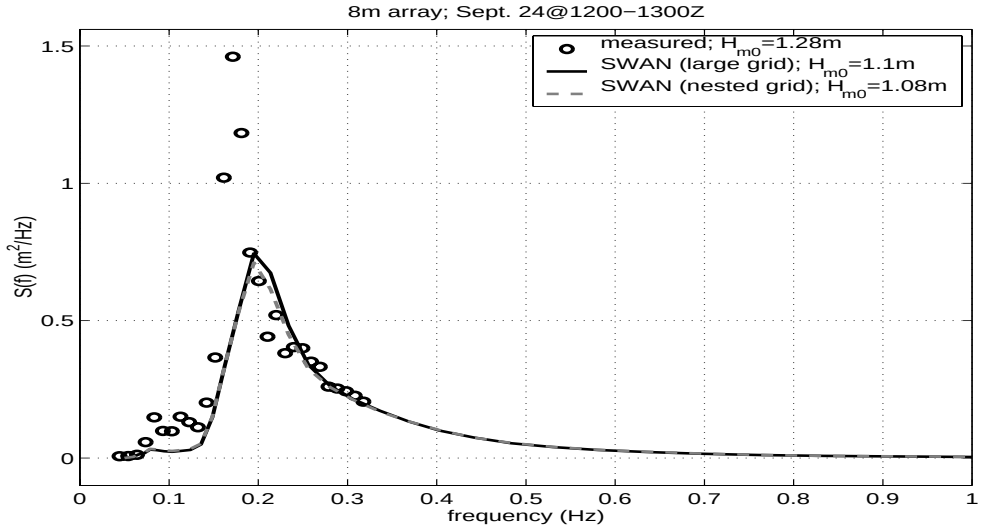

Figure 7. Frequency spectra comparison at approximately 1300 UTC 24 Sept. 1997 at the linear array (8m depth). The zero-moment waveheights, H_{m0} , given in the legend include only energy between 0.07 and 0.32 Hz. Model results the coarse resolution grid and fine grid are shown.

7. Conclusions

The most important observations and points of discussion which we make with regard to this hindcast study are the following:

1) Even with well-resolved bathymetry data (6 seconds) and even to depths as shallow as 8m, the (phase-averaged) SWAN model is much less sensitive to computational grid resolution than we would have expected. A computational grid resolution of 2km is adequate in most of the grid. Nevertheless, we believe that finer resolution would be necessary for less regular bathymetries and more swell-dominated situations.

2) We observe that total wave energy (reflected in wave height estimates) is generally well predicted, while the model poorly predicts spectral distribution of energy (reflected in low mean wave period estimates). We believe that this is due to the model's deepwater source term formulations, and not due to, e.g., inaccurate wind forcing. Further, we note that this tendency of the model is also seen in other hindcast studies.

3) We apply a modest variation of the Komen et al. (1984) dissipation formula, independently tuned for proper behavior under fully developed conditions (much like the standard Komen et al. formulation). This variation has the effect of increasing dissipation of higher frequencies, while reducing dissipation at lower frequencies. With this type of dissipation, there is an appreciable improvement in predictions of spectral distributions. However, total energy predictions are actually slightly worse. We believe this is due to the fact that this is a fetch- and duration-limited test case, whereas the dissipation term is tuned for a case of infinite fetch and duration. The form of the Komen et al. dissipation function does not have sufficient degrees of freedom to allow tuning to a more general range of conditions.

4) We observe that the presence of wind sea causes the dissipation term of SWAN to dissipate swell in a non-physical manner. We experiment with a model "switch" which disallows the breaking of swell. The experiment corrects this non-physical behavior and drastically improves model/data agreement in general. However, the manner in which swell is defined in our experiment is not entirely satisfactory. We plan to investigate other methods of treating sea and swell separately in the model, such that the presence of wind sea does not have a non-physical influence on swell, and vice versa.

Acknowledgements

This work is supported by the Office of Naval Research (Naval Research Laboratory Program Element N62435, "Phase Resolved Nonlinear Transformation of Shoaling Waves." and also the ONR Advanced Wave Prediction Program project, "Data Enhanced Modeling of Sea and Swell on the Continental Shelf"). This is NRL Contribution PP/7320-00-1016.

References

Booij, N., R.C. Ris, and L.H. Holthuijsen, 1999: A third generation wave model for coastal regions: 1. Model description and validation. J. Geophys. Res. 104, 7649-7666.

Hasselmann, K., 1974: On the spectral dissipation of ocean waves due to whitecapping. *Bound.-layer Meteor.*, **6**, 107-127.

Herbers, T.H.C., Hendrickson, E.J., and W.C. O' Reilly, 2000: Propagation of swell across a wide continental shelf. *J. Geophys. Res.* (in press).

Hwang, P.A., D. Wang, E.J. Walsh, W.B. Krabill, and R.N. Swift, 2000a: Airborne measurements of the wavenumber spectra of ocean surface waves: Part 1: Spectral slope and dimensionless spectral coefficient. *J. Phys. Oceanogr*. (in press).

Hwang, P.A., D. Wang, E.J. Walsh, W.B. Krabill, and R.N. Swift, 2000b: Airborne measurements of the wavenumber spectra of ocean surface waves: Part 2: Directional distribution. *J. Phys. Oceanogr*. (in press).

Komen, G.J., S. Hasselmann, and K. Hasselmann, 1984: On the existence of a fully developed wind-sea spectrum. *J. Phys. Oceanogr.*, **14**, 1271-1285.

Pierson, W.J., and Moskowitz, 1964: A proposed spectral form for fully developed wind seas based on the similarity theory of S. A. Kitaigorodskii. *J. Geophys. Res.* **69(24)**, 5181-5190.

Rogers, W.E., J.M. Kaihatu, N. Booij, and L. H. Holthuijsen, 1999: Improving the numerics of a third-generation wave action model. *NRL Formal Report 7320-99-9696*, 79pp.

Rogers, W.E., P.A. Hwang, D.W. Wang, and Y.L. Hsu, 2000: Investigation of wave growth and decay in a wave action model (in preparation).

Tolman, H.L., and D. Chalikov, 1996: Source terms in a third-generation wind wave model. *J. Phys. Oceanogr.*, **26**, 2497-2518.

Vledder, G.V., 1999: Source term investigation: SWAN, Rev. 2, *Report number A162R1r2*, Alkyon, 83 pp. + figures.

WAMDI Group, 1988: The WAM model—A third generation ocean wave prediction model. *J. Phys. Oceanogr.*, **18**, 1775-1810.

Wang, D.W., and P.A. Hwang, 2000: An operational method for separating wind sea and swell from ocean wave spectra (in review).